

# RAINFALL INTENSITY-DEPENDENT INFILTRATION RATES ON RANGELAND RAINFALL SIMULATOR PLOTS

J. J. Stone, G. B. Paige, R. H. Hawkins

**ABSTRACT.** Most implementations of infiltration equations with rainfall-runoff models use a hydraulic conductivity parameter that is constant for a given rainfall event. However, plot data from rainfall simulator experiments and natural rainfall events have shown that infiltration rates can increase with increasing rainfall rate instead of decreasing with time or infiltrated depth, as predicted by infiltration models. This has been hypothesized to be a function of the spatial variability of the infiltration capacity across the area. In this article, an exponential model relating steady-state infiltration rate with rainfall intensity and the average areal infiltration rate when the area under consideration is contributing to runoff is evaluated using data from variable-intensity rainfall simulator experiments. The experiments were conducted on five rangeland vegetation-soil associations at the Walnut Gulch Experimental Watershed in southeastern Arizona. The results from 19 rainfall simulation runs show that the increase in infiltration rate with increasing rainfall intensity can be significant and that the exponential model represents the relationship between steady-state infiltration and rainfall intensity. The exponential model coupled with a kinematic wave model also represents the hydrographs better than the Green-Ampt Mein-Larsen infiltration model coupled with the same routing model. The time to the start of runoff is influenced more by rainfall intensity than by initial soil moisture conditions, particularly when the initial rainfall intensity was high. The rapid time to steady-state runoff at the beginning of the simulation run of the observed runoff hydrographs suggests that the infiltration rates become constant more quickly than infiltration theory would suggest.

**Keywords.** Infiltration, Partial area response, Rainfall intensity, Rainfall simulation, Runoff.

Most applications of rainfall runoff models use a rainfall intensity-invariant parameter for infiltration. However, an increase in steady-state infiltration rate with increasing rainfall intensity has been observed by Hawkins (1982), Dunne et al. (1991), Morin and Kosovsky (1995), Janeau et al. (1999), Paige (2000), Gomez et al. (2001), Holden and Burt (2002), Mertz et al. (2002), and Paige et al. (2002). One reason put forth for the increase in infiltration rate is that there is a distribution of infiltration capacity for a given area, which is a measure of the spatial variability of soils and vegetation of that area. At a single application rate, only those areas that have an infiltration capacity less than the rainfall rate will contribute to runoff. As the intensity increases, more of the area will begin to contribute to runoff. These newly contributing areas have higher infiltration capacities, and thus the apparent infiltration rate, the rate that is measured at the point of interest, increases. On U.S. western rangelands, differences in infiltration capacity at the plot scale have been shown on

shrub sites where the infiltration rates under canopy areas are significantly higher than outside the canopy (Lyford and Qashu, 1969; Blackburn et al., 1975; Johnson and Gordon, 1988; Balliette et al., 1986). At the small watershed scale in Arizona, partial area response of runoff has been demonstrated by Artega and Rantz (1973), Lane and Wallace (1976), and Lane et al. (1978).

The effect of the intensity-invariant effective conductivity parameter,  $K_e$  (L/T), of the Green-Ampt Mein Larsen (GAML) model (Mein and Larsen, 1973) was discussed by Stone and Paige (2003) and is illustrated in figure 1. The rainfall and runoff data shown are from a rotating boom rainfall simulator experiment (Simanton and Emmerich, 1994) on a  $3 \times 10$  m plot at the USDA-ARS Walnut Gulch Experimental Watershed (WGEW) in southeastern Arizona. The plot has a gravely sandy loam surface texture and a grass-dominated vegetation community, and the data are for very wet initial soil moisture conditions. The rainfall rates were 60 and 126 mm h<sup>-1</sup>. The observed steady-state infiltration rates were computed as the difference between the rainfall rate and the observed steady-state runoff rate. The predicted infiltration and runoff rates were computed using the IRS model (Stone et al., 1992), which couples the GAML equation with a method of characteristics solution of the kinematic wave model. The GAML  $K_e$  was adjusted until the computed runoff volume matched the observed volume (Alberts et al., 1995). Note that the observed infiltration rate is larger for the higher rainfall rate, and the predicted hydrograph underpredicts discharge at the initial intensity and overpredicts the discharge at the higher intensity. This has also been documented by Paige et al. (2002).

---

Submitted for review in April 2006 as manuscript number SW 6435; approved for publication by the Soil & Water Division of ASABE in December 2007.

The authors are **Jeffrey J. Stone**, Hydrologist, USDA-ARS Southwest Watershed Research Center, Tucson, Arizona; **Ginger B. Paige**, Assistant Professor, Department of Renewable Resources, University of Wyoming, Laramie, Wyoming; and **Richard H. Hawkins**, Professor, Water Resources Program, School of Natural Resources, University of Arizona, Tucson, Arizona. **Corresponding author:** Jeffrey J. Stone, USDA-ARS-SWRC, 2000 E. Allen Rd., Tucson, AZ 85711; phone: 520-670-6381; fax 520-670-5550; e-mail: jstone@tucson.ars.ag.gov.

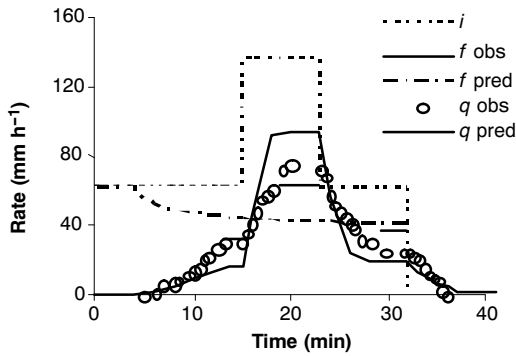


Figure 1. Observed and predicted infiltration and runoff for a multi-intensity rainfall simulator run ( $i$  = rainfall,  $f$  = infiltration,  $q$  = runoff, obs = observed, pred = predicted).

At the plot scale and larger, infiltration is not measured directly but is calculated as the difference between the rainfall and runoff rates when the latter is at steady state. The steady-state runoff rate is used because of the lag time between local rainfall excess and what is measured at the end of the plot. The runoff rate,  $q$  (L/T), of an area under consideration can be written as:

$$q(i) = \int_0^i (i - f) g(w) dw \quad (1)$$

where

- $i$  = rainfall intensity (L/T)
- $f$  = infiltration rate (L/T)
- $g(w)$  = probability density function of  $f$ .

Hawkins (1982) assumed an exponential distribution for  $g(w)$  in equation 1 and derived the following expression for the steady-state apparent infiltration rate,  $f_s$  (L/T), as a function of the rainfall intensity and the average infiltration rate,  $\mu_f$  (L/T), when the entire area under consideration is contributing to runoff:

$$f_s = \mu_f \left( 1 - e^{-\frac{i}{\mu_f}} \right) \quad (2)$$

The contributing area of runoff ( $A_c$ ) is the cumulative density function of  $G(w)$  or:

$$A_c = 1 - e^{-\frac{i}{\mu_f}} \quad (3)$$

Equation 2 was evaluated by Hawkins (1982) for a set of rainfall simulator runoff plot data using a least squares optimization of  $\mu_f$  and reproduced the observed steady-state infiltration rates very well. Although the choice of the exponential distribution was both for illustrative purposes and ease of integration of equation 1, other data (Yu et al., 1997; Yu, 1999; Paige et al., 2002) also appear to follow an exponential distribution. Yu (1999) implemented equation 2 with a rainfall excess routing method by incorporating an initial abstraction and a runoff lag parameter to compute natural rainfall runoff hydrographs on fallow plots ranging in size from 20 to 216 m<sup>2</sup>. Equation 2 performed better than the GAML model coupled with the same runoff routing routine in reproducing the runoff hydrograph. Paige (2000) and Paige et al. (2002) conducted rainfall simulations using a variable-intensity rainfall simulator on 2 × 6.1 m plots on a grassland hillslope at WGEW. Although equation 2 was not used, the

steady-state infiltration rates increased with increasing rainfall rates. Fentie et al. (2002) evaluated eight different methods of computing runoff rates using data from bare and grassed plots (30 to 340 m<sup>2</sup>) in Australia and found that equation 2 as implemented by Yu et al. (1997) performed best if a low number of data input and parameters are a concern.

Equation 2 coupled with a runoff routing method is essentially a steady-state rainfall excess model in which the rainfall excess rate is a function of the rainfall intensity. At the plot scale under natural rainfall, runoff rarely reaches steady state because of the natural variability of rainfall and the runoff lag time. Although the results of Yu et al. (1997) and Yu (1999) are the most extensive test of equation 2, they were obtained using natural rainfall. The objectives of this study are to test if equation 2 is applicable under controlled conditions in which steady-state runoff is obtained and to test if equation 2 is an improvement over the soil physics-based approach of the GAML model.

## METHODS AND MATERIALS

A variable-intensity rainfall simulator was used to generate steady-state infiltration rates at multiple rainfall intensities on 2 × 6.1 m natural vegetation rangeland plots. The  $\mu_f$  parameter in equation 2 was fit to the rainfall intensity/infiltration pairs. Hydrographs were computed by coupling equation 2 with a kinematic wave runoff routing model/method. These hydrographs were then compared with those computed using the IRS model, which uses the GAML equation and the same routing method.

### SITE DESCRIPTION

The field research for this study was conducted on the USDA-ARS WGEW located within the San Pedro River basin in southeastern Arizona. The 152 km<sup>2</sup> WGEW is a semi-arid brush-grassland complex in the transition zone between the Sonoran and Chihuahuan deserts (Renard et al., 1993). Rainfall is characterized by short duration, limited areal extent, high intensity thunderstorms, which cause most of the annual runoff in the summer months, and long duration, low intensity frontal air mass rainfall over large areas, which produces little runoff during the winter months. Five soil-vegetation associations, termed Ecological Sites (USDA, 1997), were selected for the experiment. Ecological Sites are a classification scheme used by the USDA Natural Resource Conservation Service (NRCS) in the evaluation and planning process for rangelands. An Ecological Site is defined by the soil type, depth of the top soil horizon, vegetation community, position on the landscape, and climate. Characteristics of the five sites are listed in table 1. The majority of the soils have a gravely sandy loam surface texture.

### RAINFALL SIMULATOR EXPERIMENTS

The Walnut Gulch Rainfall Simulator, a computer-controlled variable-intensity rainfall simulator (Paige et al., 2003) was used in the study. The simulator has a central oscillating boom 6 m long with four VeeJet 80100 nozzles attached at 1.52 m intervals and can apply intensities between 25 and 176 mm h<sup>-1</sup> over a 2 × 6.1 m plot. A computer is used to control a stepper motor, which controls the rate that the sprinklers move across the plot and the duration that they spray on and off the plot. The duration that the sprinklers

**Table 1. Characteristics of the Ecological Sites.**

Ecological Site	Soil Map Unit (surface textural class)	Dominant Vegetation	Average Slope
Loamy Upland	Elgin-Stronghold (gravely fine sandy loam)	black grama ( <i>Bouteloua eriopoda</i> ), hairy grama ( <i>B. hirsuta</i> ), burrowweed ( <i>Isocoma tenuisecta</i> )	11%
Limy Slopes	Elgin-Stronghold (gravely fine sandy loam)	black grama, blue three-awn ( <i>Aristida purpurea</i> ), yucca ( <i>Yucca elata</i> ), false mesquite ( <i>Calliandra eriophylla</i> )	13.5%
Limy Upland	McNeal (gravely sandy loam)	tarbush ( <i>Flourensia cernua</i> ), whitethorn ( <i>Acacia constricta</i> ), creosote ( <i>Larrea tridentata</i> )	13.5%
Sandy Loam Upland Deep	Combate (loamy sand)	plains lovegrass ( <i>Eragrostis intermedia</i> ), rothrock grama ( <i>B. rothrockii</i> ), alkali sacaton ( <i>Sporobolus airoides</i> )	3%
Clay Loam Upland	Epitaph (clay/clay loam)	tobosa ( <i>Hilaria mutica</i> ), whitethorn	9%

spray off the plot determines the application rate, with longer durations corresponding to low intensities and short durations corresponding to higher intensities. The simulator is surrounded by windbreaks on three sides to minimize the effects of wind on spray drift.

Simulations were conducted on all of the sites in 2002. At the Limy Upland site, simulations were conducted in April and June 2002, and an additional simulation run was conducted in June 2003. All of the sites had at least two simulator runs: a dry run under initial soil moisture conditions, and a wet run about 1 h after the dry run. A very wet run consisting of a series of individual rainfall rates was done on the Loamy Upland and Limy Upland sites in 2002. For all the variable-intensity runs, each rainfall rate was applied until steady-state runoff was maintained for a minimum of 5 min, and then the next rainfall intensity was applied. The targeted intensities applied were 176, 153, 123, 100, 76, and 52 mm h<sup>-1</sup>. The sequence of the intensities varied from site to site, with some runs starting with the highest intensity and others starting with the lowest. For the individual runs (termed individual high in table 2), a single intensity was run until runoff was at steady state for 5 min, at which time the rainfall simulator was shut off. When no ponded water was visible on the soil surface, the next rainfall intensity was applied. All of the individual runs started with the highest intensity. Table 2 summarizes the sequence of intensities used in the experiment. Runoff depths were measured at the end of the plot using either an electronic staff gauge or an ISCO 4200 flow depth gauge attached to a pre-calibrated flume. The runoff depths

were converted to discharge rates using the flume rating curve and the entire plot area (Simanton et al., 1991).

Detailed measurements of surface and vegetative cover were made on each plot at 480 points on a 10 × 25 cm grid using the point-line method (Bonham, 1989). At each measurement location, a pointer was dropped straight down and the canopy cover, if any, and surface cover were identified. The surface cover characteristics were classified as soil, litter, basal, gravel, or rock. The vegetative canopy cover was classified as shrub, forb, grass, or none. Ecological Site descriptions and soil series names were identified by NRCS range and soil scientists.

#### CALCULATION OF INFILTRATION PARAMETERS

In order to minimize the effects of changing soil moisture during a run, the rainfall intensity/steady-state infiltration rate pairs from the wet variable-intensity run were used to compute the infiltration parameters for both models. The steady-state infiltration rate was calculated as the difference between the rainfall intensity and the steady-state runoff for that intensity. The  $\mu_f$  parameter value (eq. 2) was determined by minimizing the root mean squared error. In order to compute the hydrograph, equation 2 was coupled with the kinematic wave routing method used in IRS (Stone et al., 1992); the coupled model is termed the exponential model in this article. The GAML effective hydraulic conductivity parameter ( $K_e$ ) was computed by adjusting its value until the simulated and observed runoff volumes matched (Alberts et al., 1995). The matric potential term of the GAML equation was estimated from the soil texture and Rawls et al. (1982). Porosity was computed from measured bulk density, and initial soil moisture was computed using soil moisture samples or in the case of missing data, estimated using data from previous rainfall simulator experiments (Simanton et al., 1991, Simanton and Emmerich, 1994). Hydrographs were computed using the optimized  $K_e$  values with the IRS model.

The goodness-of-fit for both the exponential and IRS models for the steady-state runoff rates for each plot individually was computed using the root mean squared error (RMSE, mm h<sup>-1</sup>) and the Nash-Sutcliffe efficiency coefficient ( $E$ ; Nash and Sutcliffe, 1970). The goodness-of-fit for the observed versus simulated steady-state discharge rates for all the plots as a group were evaluated using regression analysis.

**Table 2. Number of plots and rainfall intensity application sequence for the Ecological Sites (high = 176 to 52 mm h<sup>-1</sup>, low = 52 to 176 mm h<sup>-1</sup>, constant = 52 mm h<sup>-1</sup>, and individual high = discrete runs from 176 to 52 mm h<sup>-1</sup>).**

Ecological Site	No. of Plots	Intensity Sequence		
		Dry	Wet	Very Wet
Loamy Upland	2	High	High	Individual high
Limy Slopes	3	Constant	Low	
Limy Upland	5	High	High	
	3	Constant	Low	Individual high
Sandy Loam Upland Deep	3	Constant	High	
Clay Loam Upland	1	Constant	High	
	2	Constant	Low	

## RESULTS

### MEASUREMENTS

Ground cover ranged from 82% for the Loamy Upland site to 36% for the Sandy Loam Upland Deep site (table 3). Surface gravel was highest on the Limy Upland site (67%) and totally absent on the Sandy Loam Upland Deep site. Canopy cover followed the same trend, with the Loamy Upland site having the highest amount of canopy cover (88%) and the Sandy Loam Upland Deep site having the lowest with 39%. Grass cover was the dominant canopy for all of the sites except the Limy Upland site, which essentially has no grass. The Clay Loam Upland site was singular in the fact that the rocks on the soil surface and within the soil profile were larger (up to 48 cm in diameter) than at the other sites, and extensive cracks extending from the soil surface to 24 to 48 cm below were observed.

The full range of target rainfall intensities was not attained on several of the simulation runs due to equipment failures. However, data from these runs were included in the analysis if the number of intensities was sufficient to define the relationship between rainfall intensity and  $\mu_f$ . Table 4 summarizes the hydrologic variables, including the runoff ratio, time from the beginning of the run to the start of runoff, and time to the first steady-state discharge rate. The runoff ratios ranged from a low of 0.29 at the Loamy Upland site to about 0.70 at the Limy Slopes, Limy Upland, and Clay Loam Upland sites.

The time to the start of runoff for all the sites was less than 6 min. There was a strong relationship between the time to the start of runoff ( $t_r$ ) and the initial rainfall intensity ( $i_0$ ). Using the individual run data for the Loamy Upland and Limy Upland 2003 sites, the site average  $t_r$  is plotted versus  $i_0$  in figure 2. The data follow a non-linear relationship, with  $t_r$  decreasing rapidly as the intensity increases and leveling off around 100 mm h<sup>-1</sup>. The data for the dry and wet variable-intensity runs did not have enough points to define a relationship, as there was only one initial intensity for each run. However, there were enough runs that started at a high intensity and others that started at a low intensity to demonstrate that the trend was similar to that of the individual runs. Referring to figure 3, the  $t_r$  values for the dry run show a larger range when the initial rainfall intensity was low and much less when it was high. For the wet run, the range of  $t_r$  is less than the dry run for the low initial intensity, and in general the

Table 3. Ecological Site average plot cover characteristics.<sup>[a]</sup>

Ecol. Site <sup>[b]</sup>	Ground Cover (%)				Canopy Cover (%)			
	R	L	B	Total	G	S	F	Total
LoU	26	41	16	82	63	13	13	88
	(27)	(12)	(34)	(9)	(31)	(63)	(59)	(4)
LS	33	20	8	60	34	6	24	64
	(21)	(7)	(10)	(7)	(23)	(150)	(1)	(2)
LU	67	7	6	78	1	37	9	48
	(7)	(95)	(98)	(7)	(91)	(32)	(44)	(31)
SLUD	0	33	3	36	24	11	4	39
	(0)	(2)	(1)	(2)	(36)	(25)	(114)	(41)
CLU	27	28	5	64	42	6	0	48
	(72)	(92)	(61)	(2)	(81)	(11)	(0)	(69)

<sup>[a]</sup> R = rock, L = litter, B = vegetation base, G = grass, S = shrub, and F = forb; values in parentheses are coefficients of variation (%).

<sup>[b]</sup> LoU = Loamy Upland, LS = Limy Slopes, LU = Limy Upland, SLUD = Sandy Loam Upland Deep, CLU = Clay Loam Upland.

Table 4. Hydrological variables for the wet run.<sup>[a]</sup>

Ecol. Site <sup>[b]</sup>	Plot	P (mm)	Q (mm)	Q/P	$t_r$ (min)	$t_e$ (min)
LoU	4	125	45	0.42	1.73	9.0
	5	96	28	0.29	1.42	8.0
LS	3	151	83	0.55	5.00	9.5
	7	141	98	0.70	4.50	7.0
	8	91	39	0.42	3.25	7.0
LU	1a <sup>[c]</sup>	57	33	0.58	1.27	4.5
	1j	91	67	0.73	1.13	4.5
	2a	97	53	0.54	1.37	3.5
	2j	84	59	0.71	0.98	2.5
	5a	95	49	0.52	0.75	4.0
	1y	114	63	0.55	3.71	8.0
	2y	89	67	0.75	1.62	5.5
	3y	112	50	0.44	3.28	5.0
SLUD	1	114	38	0.33	1.50	4.0
	2	134	73	0.54	0.93	5.0
	3	118	68	0.57	1.18	6.0
CLU	1	200	89	0.44	2.83	44.0
	4	115	70	0.61	5.93	30.0
	6	83	58	0.70	2.60	6.0

<sup>[a]</sup> P = total rainfall, Q = total runoff,  $t_r$  = time to runoff, and  $t_e$  = time to steady-state runoff at the initial rainfall intensity.

<sup>[b]</sup> LoU = Loamy Upland, LS = Limy Slopes, LU = Limy Upland, SLUD = Sandy Loam Upland Deep, CLU = Clay Loam Upland.

<sup>[c]</sup> Simulations done in a = April, j = June, y = 2003.

values of  $t_r$  are lower for both the high and low initial intensities. For all of the sites with the exception of the Clay Loam Upland site, steady-state runoff for the initial intensity was reached on average by 4 min ( $t_e - t_r$  in table 4). The Clay Loam Upland site had a significant amount of depression storage that retarded the time to steady-state runoff. For plot 1, steady-state runoff occurred 44 min into the run with an initial rainfall intensity of 176 mm h<sup>-1</sup>, and plot 4 did not reach steady-state runoff until the third rainfall rate, which was 30 min into the run.

### PARAMETERS VALUES

The optimized parameter values for  $\mu_f$  and  $K_e$  are given in table 5. The range of  $\mu_f$  was considerable within an Ecological Site, varying by as much as 80 mm h<sup>-1</sup> for the Sandy Loam Upland Deep site and 70 mm h<sup>-1</sup> for the Loamy Upland Site. The mean  $\mu_f$  values for each site followed an expected

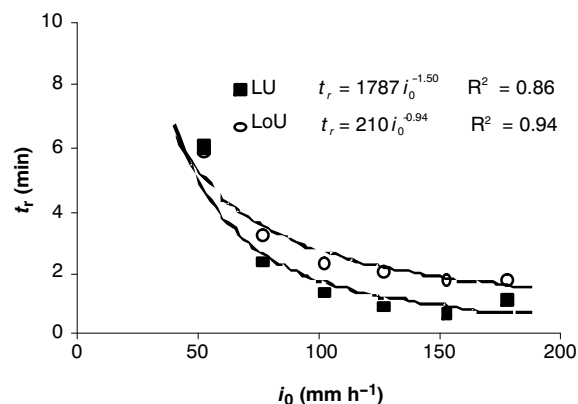
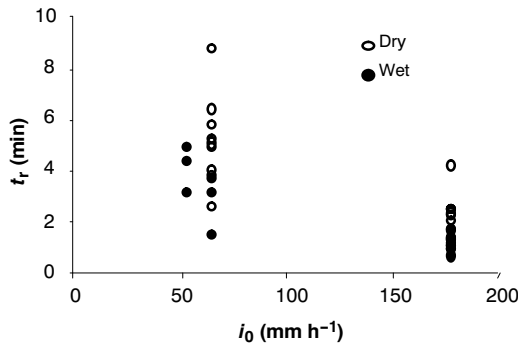


Figure 2. Site average relationship between the time to runoff ( $t_r$ ) and initial rainfall intensity ( $i_0$ ) for the individual intensity runs for the Loamy Upland (LoU) and Limy Upland (LU) sites.



**Figure 3. Relationship between time to runoff ( $t_r$ ) and initial rainfall intensity ( $i_0$ ) for all the sites for the dry and wet variable-intensity runs.**

trend, with the sandier sites having higher values and the clay site having the lowest value. However, the small number of plots for most of the sites with the high variability of response resulted in no statistical difference in the mean values of  $\mu_f$  among the sites as measured by the Tukey test ( $p \leq 0.05$ ).

Figure 4 illustrates the type of fit obtained using equation 2 with the observed rainfall intensity/steady-state infiltration pairs. For plot 8, Limy Slopes, the  $\mu_f$  value is high ( $96 \text{ mm h}^{-1}$ ), and it appears that the infiltration rate has not reached a constant value even at the highest rainfall intensity ( $176 \text{ mm h}^{-1}$ ) applied during the experiment. Using equation 3, the contributing area corresponding to  $176 \text{ mm h}^{-1}$  is 0.84, meaning that 16% of the plot had an infiltration capacity larger than  $176 \text{ mm h}^{-1}$ . In contrast, the infiltration rate for

plot 2, Limy Upland, appears to have reached a constant value at a relatively low rainfall rate of  $76 \text{ mm h}^{-1}$ . For this intensity, equation 3 computes a contributing area of 0.90, meaning that 10% of the plot has a higher infiltration capacity than  $76 \text{ mm h}^{-1}$ .

Using the site average  $\mu_f$ , the infiltration versus rainfall intensity and the contributing area versus rainfall intensity are computed and plotted in figures 5 and 6, respectively, for all of the sites. The Loamy Upland and Sandy Loam Upland sites do not approach a constant infiltration value at the highest intensities while the remainder of the sites do approach a constant value (fig. 5). In figure 6, the range of contributing area is greatest at the moderate intensities and decreases as the intensity decreases or increases from the intensity of maximal difference. For example, at a rainfall intensity of  $60 \text{ mm h}^{-1}$ , the range of contributing area is less than 0.40 for the Loamy Upland site to about 0.75 for the Clay Loam Upland site. At a rainfall intensity of  $176 \text{ mm h}^{-1}$ , the range is about 0.75 to 0.99 for the same sites.

The values of  $K_e$  followed a similar trend, although the variability of the parameter values within a site was less than for  $\mu_f$  and the magnitude of the values was uniformly lower. Using fallow plot natural rainfall-runoff data, Yu (1999) developed the following second-order polynomial relationship:  $\log \mu_f = 0.534 + 0.316(\log K_e) + 0.402(\log K_e)^2$  (equation 10 in Yu, 1999). For comparison, the  $K_e$  and  $\mu_f$  from this study were found to be best fit by the following exponential model:

$$\mu_f = 24 e^{0.0304 K_e} \quad R^2 = 0.85 \quad (4)$$

**Table 5. Parameter values and goodness-of-fit statistics for steady-state runoff for the exponential and IRS models. RMSE is the root mean squared error, and  $E$  is the Nash-Sutcliffe efficiency coefficient.**

Ecological Site <sup>[a]</sup>	Plot	Exponential Model			IRS Model		
		$\mu_f$ ( $\text{mm h}^{-1}$ )	RMSE ( $\text{mm h}^{-1}$ )	$E$	$K_e$ ( $\text{mm h}^{-1}$ )	RMSE ( $\text{mm h}^{-1}$ )	$E$
LoU	4	87	6.59	0.96	37	10.19	0.93
	5	157	3.70	0.97	50	10.31	0.89
	Mean (CV)	122 (41)			44 (21)		
LS	3	66	3.57	0.99	35	16.15	0.88
	7	35	4.32	0.99	17	11.94	0.94
	8	96	4.14	0.98	40	20.79	0.79
	Mean (CV)	66 (46)			31 (39)		
LU	1a <sup>[b]</sup>	51	6.31	0.98	17	3.34	0.99
	1j	27	6.88	0.98	9	4.50	0.99
	2a	63	3.44	0.99	23	9.73	0.93
	2j	30	7.18	0.98	10	4.50	0.99
	5a	63	4.96	0.98	26	9.33	0.93
	1y	57	2.86	0.99	28	15.20	0.90
	2y	28	3.59	0.99	10	8.63	0.96
	3y	85	6.36	0.95	40	15.66	0.89
	Mean (CV)	51 (41)			20 (54)		
SLUD	1	140	5.64	0.95	61	15.45	0.83
	2	58	2.32	1.00	36	3.76	0.99
	3	58	1.94	1.00	30	2.52	0.98
	Mean (CV)	85 (55)			42 (39)		
CLU	1	60	11.68	0.89	47	22.01	0.70
	4	38	21.04	0.74	16	15.36	0.91
	6	33	8.50	0.96	8	16.01	0.89
	Mean (CV)	44 (33)			24 (87)		

<sup>[a]</sup> LoU = Loamy Upland, LS = Limy Slopes, LU = Limy Upland, SLUD = Sandy Loam Upland Deep, CLU = Clay Loam Upland.

<sup>[b]</sup> Simulations done in a = April, j = June, y = 2003.

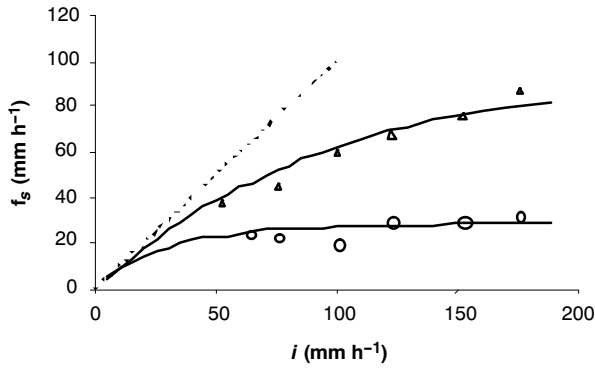


Figure 4. Wet run steady-state infiltration rate ( $f_s$ ) versus rainfall intensity ( $i$ ) for plot 8, Limy Slopes site (triangles) and plot 2, 2003 Limy Upland site (circles). Solid lines are equation 2, and dashed line is the 1:1 line.

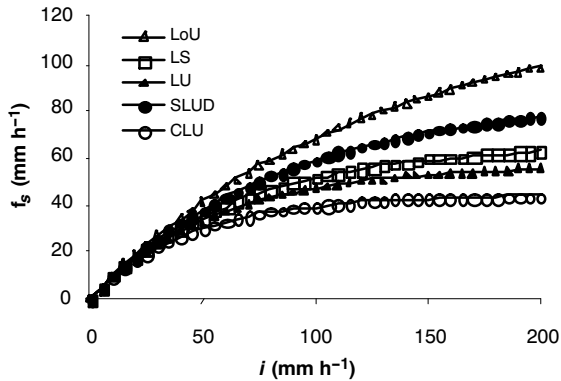


Figure 5. Ecological Site average steady-state infiltration ( $f_s$ ) versus rainfall intensity ( $i$ ): LoU = Loamy Upland, LS = Limy Slopes, LU = Loamy Upland, SLUD = Sandy Loam Upland Deep, and CLU = Clay Loam Upland.

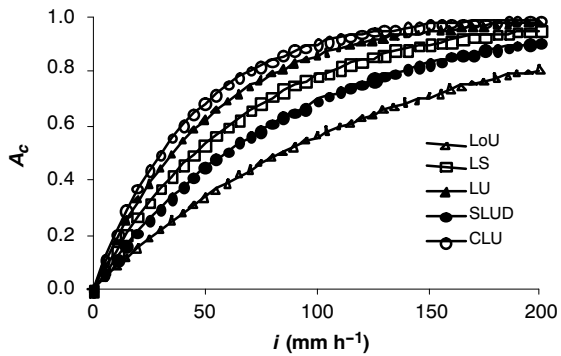


Figure 6. Ecological Site average contributing area ( $A_c$ ) versus rainfall intensity ( $i$ ): LoU = Loamy Upland, LS = Limy Slopes, LU = Loamy Upland, SLUD = Sandy Loam Upland Deep, and CLU = Clay Loam Upland.

Plotted in figure 7 are the data pairs from this study, equation 4 and equation 10 from Yu (1999).

Stepwise multiple linear regressions were done using  $\log_e$  transforms of  $\mu_f$  and  $K_e$  and the variables in table 3. The resulting equations are listed in table 6. Both basal cover and bare soil were positively correlated with  $\mu_f$  when the entire data set was used in the regression. A positive correlation with bare soil conflicts with previous studies at WGEW that have shown a significant negative correlation between bare soil and runoff and erosion (Simanton and Renard, 1982; Simanton et al., 1991; Simanton and Emmerich, 1994). A sec-

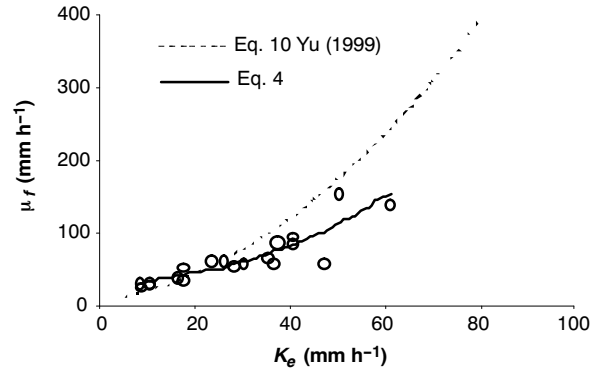


Figure 7. Relationship between  $\mu_f$  and  $K_e$ .

Table 6. Cover relationships for  $\mu_f$  and  $K_e$ .

Equation	$r^2$	rmse <sup>[a]</sup> ( $\text{mm h}^{-1}$ )
$\ln(\mu_f) = 3.02 + 0.081 \text{ Basal} + 0.016 \text{ Soil}$	0.47	21
$\ln(\mu_f) = 4.06 - 0.018 \text{ Rock} + 0.074 \text{ Basal}^{\text{[b]}}$	0.73	21
$\ln(K_e) = 2.59 + 0.029 \text{ Litter}$	0.36	12

[a] Root mean squared error for untransformed dependent variable.

[b] Without the Limy Upland site.

ond regression analysis was done without the Limy Upland site, which increased the correlation coefficient and resulted in coefficients that are more consistent with previous work. Litter was the only variable correlated with  $K_e$  when the entire data set was used, and the correlation coefficient was lower than for both the  $\mu_f$  equations. The correlation coefficient decreased when the Limy Upland site was removed from the analysis.

## HYDROGRAPHS

The exponential and IRS models both predicted the steady-state discharge rate accurately, as evidenced by the high Nash-Sutcliffe  $E$  values (table 5). For the exponential model,  $E$  was close to 1 for all of the sites, with the exception of two plots at the Clay Loam Upland site, and was generally higher than those for the IRS model. The RMSE also was generally lower for the exponential model than for IRS. Figure 8 is a plot of observed versus simulated steady-state discharge for the two models. Both models have high correlation coefficients, and at the 95% level, the slopes are not significantly different from 1 and the intercepts are not significantly different from 0 (fig. 8).

Examples of observed and predicted hydrographs are plotted for the exponential (fig. 9a) and IRS (fig. 9b) models for plot 8 of the Loamy Upland site, a run with a low initial rainfall intensity. The exponential model underpredicted the start of runoff and generally follows the observed hydrograph. Note that the simulated runoff actually starts at time zero, but because of the lag time, does not reach significant levels until several minutes into the run. The IRS model significantly overpredicted the time to runoff, thus underestimating the low runoff rates and overpredicting the higher rates. For the runs that started with a low intensity, on average the IRS model underpredicted the time to start of runoff by about 9 min. Both models did well when the initial intensity was high, as for plot 2, Limy Uplands 2003 (fig. 10). Even though the exponential model does not have an initial abstraction term, the simulated hydrograph matched the time to

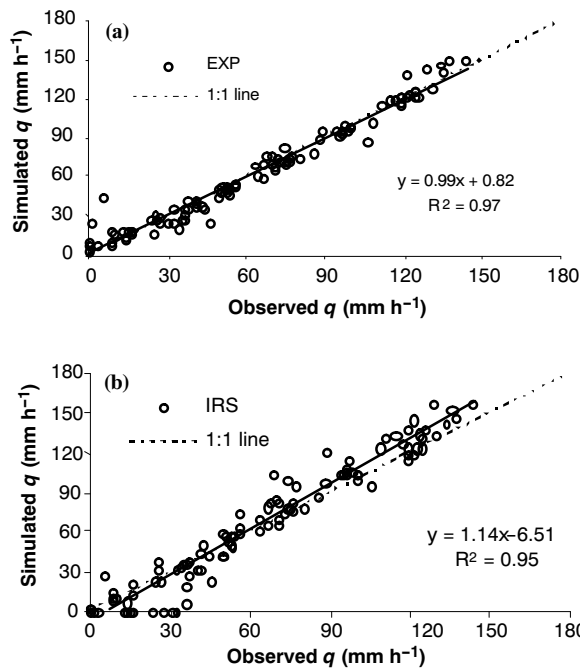


Figure 8. Observed versus simulated steady-state runoff ( $q$ ) for all rainfall intensities for all the sites for (a) the exponential model and (b) the IRS model.

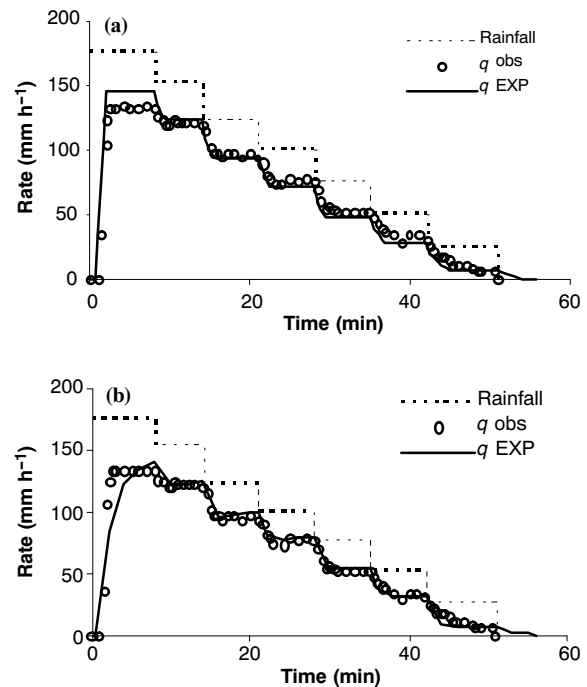


Figure 10. Observed and simulated wet run hydrograph for plot 2y 2003, Limy Upland site for (a) the exponential model and (b) the IRS model ( $q_{obs}$  = observed runoff,  $q_{EXP}$  = exponential model, and  $q_{IRS}$  = IRS model).

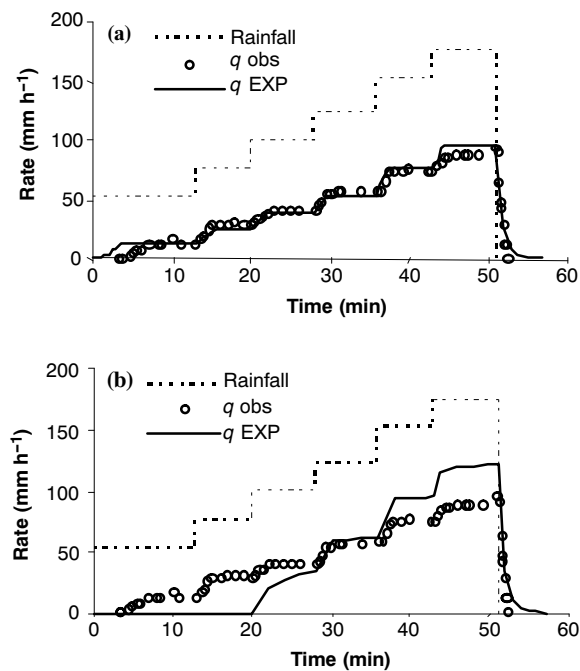


Figure 9. Observed and simulated wet run hydrograph for plot 8, Limy Slopes site for (a) the exponential model and (b) the IRS model ( $q_{obs}$  = observed runoff,  $q_{EXP}$  = exponential model, and  $q_{IRS}$  = IRS model).

start of runoff and the hydrograph rise very well, although it overestimated the initial peak runoff rate. The IRS model also did well in matching the observed time to start of runoff and hydrograph, but it did not reach steady state at the initial rainfall intensity.

## DISCUSSION

The results show that accounting for the effect of rainfall intensity on the runoff process using a rainfall intensity-dependent infiltration relationship is an improvement over a conventional intensity-invariant approach such as the IRS model, at least at the plot scale. The IRS model shows a bias, underpredicting low discharge rates and overpredicting higher discharge rates (fig. 8), which the exponential model does not. Both models had relatively high goodness-of-fit statistics, although the statistics for the exponential model on average were better. Part of the success of both models is that the goodness-of-fit was based on matching the steady-state discharge and not the entire hydrograph. However, the exponential model will accurately reproduce the steady-state discharge rates if equation 2 accurately represents the rainfall intensity/infiltration relationship because of the small lag time between the steady-state rainfall excess and runoff rates at the plot scale. For the IRS model, even for wet moisture conditions, the computed infiltration rates only approach steady state. If the infiltration/rainfall intensity relationship quickly approaches a constant value, as does plot 2, Limy Uplands (fig. 10), then the computed hydrographs should match the observed.

The behavior of the IRS-computed hydrograph compared to the observed during the beginning of a run offers an important point of discussion. The observed hydrographs at the beginning of the simulation runs reach steady state relatively quickly (table 5) and, as shown in figures 9 and 10, show the same behavior for subsequent rainfall intensities, a rapid rise and a flat-topped hydrograph. In contrast, the IRS model hydrographs approach steady-state runoff more slowly at the beginning of an event and for several rainfall intensities following the initial intensity. The reason for this is that after the time to ponding at the beginning of a simulation run, the

GAML model will predict a decrease in the infiltration rate, which will approach a constant value as a function of the initial soil moisture and cumulative infiltration. The rate of the decrease at the beginning is primarily a function of soil moisture such that for dry soil moisture conditions, the decrease is slower than for wet conditions. The result is that the rise of the GAML hydrograph has the characteristic shape shown in figures 9b and 10b and often does not reach steady state. That the observed hydrographs do not show this characteristic shape suggests that they are a result of constant rainfall excess and that the theoretical infiltration curve does not apply. In this case, application of the exponential model with a runoff routing method should result in a very good approximation of the runoff process at the plot scale.

Most methods to compute runoff incorporate an initial abstraction before runoff occurs. The curve number method (USDA, 1985) assumes a rainfall depth that is a function of a retention factor as an initial abstraction from the total storm rainfall. Mein and Larsen (1973) modified the Green-Ampt equation to incorporate time to ponding as a function of the Green-Ampt parameters, initial soil moisture, and rainfall intensity. In applying equation 2 with natural rainfall-runoff events, Yu et al. (1999) included an initial abstraction term that was calibrated to fit the hydrographs of the plot data used in the study and developed an empirical relationship to estimate the term based on the GAML parameters. The relationships shown in figures 2 and 3 suggest that rainfall intensity is the dominant factor in determining when runoff starts. In figure 3,  $t_r$  for the lower initial intensities has a wider range for the dry moisture condition but is within the range of the wet moisture condition. When the initial rainfall intensity is high, the difference between the dry and wet  $t_r$  is on the order of a couple of minutes. For several plots, runoff ceased at the lowest rainfall intensity, but ponding was observed on areas of the plot, indicating that the rainfall rate was higher than the infiltration capacity for those areas. That those local areas of rainfall excess did not produce runoff could be due to the runoff-runon process or that the infiltration rate was greater than the rate needed to fill depression storage. This suggests that these two processes may be a factor in determining initial abstraction. In any case, the small times to the start of runoff indicate that not accounting for an initial abstraction at this scale may not cause much error in the computed hydrograph.

As mentioned at the beginning of this article, the increase in infiltration rate with rainfall rate is hypothesized to be a function of the spatial variability of the infiltration capacity over the given area. The results of the multiple linear regression of  $\ln(\mu_f)$  for the grassland sites (table 6) suggest that the  $f_s-i$  curve is flatter when vegetation (basal cover) is less. This is consistent with other studies that compared vegetated versus bare plots in which the  $f_s-i$  curve is flatter for bare plots than vegetated plots (Hawkins, 1982; Janeau et al., 1999) and tends to be flatter as the percent vegetative cover decreases (Dunne et al., 1991). Microtopography has also been suggested as a cause of changes in infiltration with rainfall intensity, either due to plant root systems and increased hydraulic roughness causing increased flow depths that inundates areas of microtopography that have higher infiltration capacities (Dunne et al., 1991) or due to differences in the types of crusts on mounds and within interspaces (Fox et al., 1998). The interaction of vegetation and microtopography may explain why the correlation between  $\mu_f$  and cover variables increased when the Limy Upland site was not included in the regression

analysis (table 6). Mounds form under creosote bush, the dominant vegetation of the Limy Upland site, and the infiltration rate has been shown to decrease from the plant base to the interspace areas (Lyford and Qashu, 1969). It could be that the infiltration rates are controlled by different processes on different vegetation systems, as suggested by Spaeth et al. (1996) and Pierson et al. (2002). For the grassland sites of this study, crusts could also be a factor in determining infiltration rates. Obstructions to flow, including permanent litter, rocks, and vegetative bases, trap sediment, forming microterraces. During simulation runs, it has been observed that these areas tend to pond water earlier than the other areas.

Most rainfall simulator experiments are conducted using a single rainfall intensity, and the results are presented on a unit area basis with the assumption that the entire plot is contributing to runoff. The results from this study and others cited in this article suggest that for vegetated areas on coarser-textured soils, the typical rainfall simulator experimental design and assumptions of no partial area response may not be valid in the determination and quantification of infiltration processes on rangelands. Further research of this type is needed to validate these results on other rangeland vegetation communities other than those used in this study.

## SUMMARY

Infiltration models based on soil physics theory predict a decrease in the infiltration rate with time or cumulative infiltrated depth. Analysis of rainfall simulator plot data have shown that the steady-state infiltration rate either increases or is constant with increasing rainfall intensity (Hawkins, 1982; Paige, 2000). Hawkins (1982) developed an exponential model that relates steady-state infiltration rates to rainfall intensity and tested the relationship on one set of plot data. In this study, a variable-intensity rainfall simulator was used on  $2 \times 6.1$  m plots on five rangeland soil-vegetation associations in southeastern Arizona to test if the exponential model performs better than the conventional infiltration-based approach of the GAML model. Both models were coupled with a kinematic wave model to compute the runoff hydrograph. The results from all of the sites show that the exponential model performed better than the GAML model in predicting the steady-state runoff rates. Overall, the GAML model tended to underpredict the small discharge rates and overpredict the large rates. The shape of the observed hydrographs and the success of the exponential model suggest that at the plot scale, the rainfall excess rate approaches a constant value rapidly.

## REFERENCES

- Artega, F. E., and S. E. Rantz. 1973. Application of the source-area concept of storm runoff to a small Arizona watershed. *J. Research, USGS* 1(4): 493-498.
- Alberts, E. E., M. A. Nearing, M. A. Weltz, L. M. Risse, F. B. Pierson, X. C. Zhang, J. M. Lafen, and J. R. Simanton. 1995. Chapter 7: Soil component. In *Technical Documentation*, 7.28-7.34. NSERL Report No. 10. West Lafayette, Ind.: USDA Water Erosion Prediction Project (WEPP).
- Balliette, J. F., K. C. McDaniel, and M. K. Wood. 1986. Infiltration and sediment production following chemical control of sagebrush in New Mexico. *J. Range Mgmt.* 39(2): 160-165.

- Blackburn, W. H., R. E. Eckert, Jr., M. K. Wood, and F. F. Peterson. 1975. Influence of vesicular horizons on watershed management. In *Proc. Watershed Management, A Symposium*, 494-515. Reston, Va.: ASCE, Irrigation and Drainage Division.
- Bonham, C. D. 1989. *Measurements for Terrestrial Vegetation*. New York, N.Y.: John Wiley and Sons.
- Dunne, T., W. Zhang, and B. F. Aubry. 1991. Effects of rainfall, vegetation, and microtopography on infiltration and runoff. *Water Resources Res.* 27(9): 2271-2285.
- Fentie, B., B. Yu, M. D. Silburn, and C. A. A. Ciesiolka. 2002. Evaluation of eight different methods to predict hillslope runoff rates for a grazing catchment in Australia. *J. Hydrol.* 261: 102-114.
- Fox, D. M., Y. Le Bissonnais, and P. Quetin. 1998. The implications of spatial variability in surface seal hydraulic resistance for infiltration in a mound and depression microtopography. *Catena* 32(2): 101-114.
- Gomez, J. A., J. V. Giraldez, and E. Fereres. 2001. Analysis of infiltration and runoff in an olive orchard under no-till. *SSSA J.* 65(2): 291-299.
- Hawkins, R. H. 1982. Interpretations of source area variability in rainfall-runoff relations. In *Rainfall-Runoff Relationship*, 303-324. V. P. Singh, ed. Littleton, Colo.: Water Resources Publications.
- Holden, J., and T. P. Burt. 2002. Infiltration, runoff, and sediment production in blanket peat catchments: Implications of field rainfall simulation experiments. *Hydrol. Processes* 16(13): 2537-2557.
- Janeau, J. L., A. Mauchamp, and G. Tarin. 1999. The soil surface characteristics of vegetation stripes in northern Mexico and their influence on the system hydrodynamics: An experimental approach. *Catena* 37(1-2): 165-173.
- Johnson, C. W., and N. D. Gordon. 1988. Runoff and erosion from rainfall simulator plots on sagebrush rangeland. *Trans. ASAE* 31(2): 421-427.
- Lane, L. J., and D. E. Wallace. 1976. Simulation of partial area response from a small semiarid watershed. In *Proc. Joint Meetings of Arizona Section of AWRA and Hydrology Section*, 137-147. Tucson, Ariz.: Arizona Academy of Science.
- Lane, L. J., M. H. Diskin, D. E. Wallace, and R. M. Dixon. 1978. Partial area response on small semiarid watersheds. *AWRA Water Resources Bulletin* 14(5): 1143-1158.
- Lyford, F. P., and H. K. Qashu. 1969. Infiltration rates affected by desert vegetation. *Water Resources Res.* 5(6): 1373-1376.
- Mein, R. G., and C. L. Larson. 1973. Modeling infiltration during a steady rain. *Water Resources Res.* 9(2): 384-394.
- Mertz, B., A. Bardossy, and G. R. Shiffler. 2002. Different methods for modeling the areal infiltration of a grass field under heavy precipitation. *Hydrol. Processes* 16(7): 1383-1402.
- Morin, J., and A. Kosovsky. 1995. The surface infiltration model. *J. Soil and Water Cons.* 50(5): 470-476.
- Nash, J. E., and J. V. Sutcliffe. 1970. River flow forecasting through conceptual models: Part 1. A discussion of principles. *J. Hydrol.* 10(3): 282-290.
- Paige, G. B. 2000. Measurement and modeling of the spatial variability of infiltration on rangeland watersheds. PhD diss. Tucson, Ariz.: University of Arizona, School of Renewable Natural Resources.
- Paige, G. B., J. J. Stone, D. P. Guertin, and L. J. Lane. 2002. A strip model approach to parameterize a coupled Green-Ampt kinematic wave model. *JAWRA* 38(5): 1363-1378.
- Paige, G. B., J. J. Stone, J. Smith, and J. R. Kennedy. 2003. The Walnut Gulch rainfall simulator: A computer-controlled variable-intensity rainfall simulator. *Applied Eng. in Agric.* 20(1): 25-31.
- Pierson, F. B., K. E. Spaeth, M. A. Weltz, and D. H. Carlson. 2002. Hydrologic response of diverse western rangelands. *J. Range Mgmt.* 55(6): 558-570.
- Rawls, W. J., D. L. Brakensiek, and K. E. Saxton. 1982. Estimation of soil water properties. *Trans. ASAE* 25(5): 1316-1320.
- Renard, K. G. L. J. Lane, J. R. Simanton, W. E. Emmerich, J. J. Stone, M. A. Weltz, D. C. Goodrich, and D. S. Yakowitz. 1993. Agricultural impacts in an arid environment: Walnut Gulch studies. In *Proc. 2nd US/CIS Joint Conf. on Environmental Hydrology and Hydrogeology*, 9(1-4): 149-159. Smyrna, Ga.: American Institute of Hydrology.
- Simanton, J. R., and K. G. Renard. 1982. Seasonal change in infiltration and erosion from USLE plots in southeastern Arizona. *Hydrology and Water Resources in Arizona and the Southwest* 12: 37-46. Tucson, Ariz.: University of Arizona, Office of Arid Land Studies.
- Simanton, J. R., and W. E. Emmerich. 1994. Temporal variability in rangeland erosion, processes. In *Variability in Rangeland Water Erosion Processes*, 51-65. W. H. Blackburn, F. B. Pierson, G. E. Schuman, and R. Zartman, eds. SSSA Spec. Pub. No. 38. Madison, Wisc.: SSSA.
- Simanton, J. R., M. A. Weltz, and H. D. Larson. 1991. Rangeland experiments to parameterize the water erosion prediction model: Vegetation canopy cover effects. *J. Range Manage* 44(3): 276-282.
- Spaeth, K. E., F. B. Pierson, M. A. Weltz, and J. B. Awang. 1996. Gradient analysis of infiltration and environmental variables as related to rangeland vegetation. *Trans. ASAE* 39(1): 67-77.
- Stone, J. J., and G. B. Paige. 2003. Variable rainfall intensity rainfall simulator experiments on semi-arid rangelands. In *Proc. 1st Interagency Conf. on Research in the Watersheds*, 83-88. K. G. Renard, S. McElroy, W. Gburek, E. Canfield, and R. L. Scott, eds. Washington, D.C.: USDA Agricultural Research Service.
- Stone, J. J., L. J. Lane, and E. D. Shirley. 1992. Infiltration and runoff simulation on a plane. *Trans. ASAE* 35(1): 161-170.
- USDA. 1985. *National Engineering Handbook*. Section 4: Hydrology. Washington D.C.: USDA Soil Conservation Service.
- USDA. 1997. *National Range and Pasture Handbook*. 190-vi-NRPH. Washington, D.C.: USDA-NRCS Grazing Lands Technology Institute.
- Yu, B. 1999. A comparison of the Green-Ampt and a spatially variable infiltration model for natural storm events. *Trans. ASAE* 42(1): 89-97.
- Yu, B., C. W. Rose, K. J. Coughlan, and B. Fentie. 1997. Plot-scale rainfall-runoff characteristics and modeling at six sites in Australia and southeast Asia. *Trans. ASAE* 40(5): 1295-1303.

